JACS
JOURNAL OF THE AMERICAN CHEMICAL SOCIETY
Article
pubs.acs.org/JACS

The Photochemical Route to Octahedral Iron(V). Primary Processes and Quantum Yields from Ultrafast Mid-Infrared Spectroscopy

Hendrik Vennekate,[†] Dirk Schwarzer,*[,†] Joel Torres-Alacan,[‡] and Peter Vöhringer*[,‡]

[†]Max-Planck-Institut für biophysikalische Chemie, Am Fassberg 11, 37077 Göttingen, Germany

[‡]Institut für Physikalische und Theoretische Chemie, Rheinische Friedrich-Wilhelms-Universität, Wegelerstraße 12, 53115 Bonn, Germany

Supporting Information

ABSTRACT: Recently, the complex cation $[(\text{cyclam-ac})\text{Fe}^{\text{III}}(\text{N}_3)]^+$ has been used in solid matrices under cryogenic conditions as a photochemical precursor for an octahedral iron nitride containing the metal at the remarkably high oxidation state +5. Here, we study the photochemical primary events of this complex cation in liquid solution at room temperature using femtosecond time-resolved mid-infrared (fs-MIR) spectroscopy as well as step-scan Fourier-transform infrared spectroscopy, both of which were carried out with variable-wavelength excitation. In stark contrast to the cryomatrix experiments, a photooxidized product cannot be detected in liquid solution when the complex is excited through its putative LMCT band in the visible region. Instead, only a redox-neutral dissociation of azide anions is seen under these conditions. However, clear evidence is found for the formation of the highly oxidized iron nitride product when the photolysis is carried out in liquid solution with UV light. Yet, the photooxidation must compete with photoreductive Fe−N bond cleavage leading to azide radicals and an iron(II) complex. Both, redox-neutral and photoreductive Fe−N bond breakage as well as photooxidative N−N bond breakage occur on a time scale well below a few hundred femtoseconds. The majority of fragments suffer from geminate recombination back to the parent complex on a time scale of 10 ps. Upper limits of the primary quantum yield for photooxidation are derived from the fs-MIR data, which increase with increasing energy of the photolysis photon.

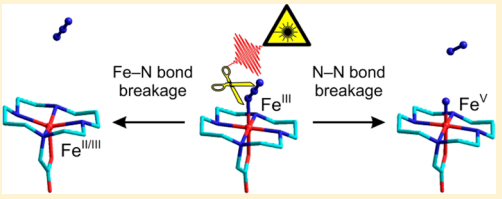

INTRODUCTION

High-valent iron, i.e., Fe-containing species with the metal center at the oxidation states +4, +5, or +6, is implicated in the catalytic cycles of a number of heme and non-heme enzymes.[1−8] A prominent example of such proteins is the cytochrome P450, which catalyzes via an iron(IV)oxo species and a rebound mechanism in the biochemical oxidation of hydrocarbons.[9,10] This prominent importance for the enzymatic oxidation has been a significant driving force for bioinorganic chemists to develop small synthetically accessible models containing highly oxidized iron in a well-defined and controllable coordination environment.[11,12] A particular emphasis was laid recently on high-valent iron complexes featuring a nitrido ligand[13] because complementary transition-metal species have been utilized for in vitro nitrogen fixation.[14,15]

Such iron nitrides turn out to be rather stable even at room temperature when the transition metal is embedded in a coordination environment with three-fold symmetry.[16−18] A tris(carbine)amine-iron(IV)-nitride was recently employed as an electrochemical precursor for a complementary iron(V) species that was stable enough for its electronic and molecular structure to be examined by crystallography and various types of spectroscopy.[19,20] Quite in contrast, iron nitrides with a four-fold symmetrical coordination geometry at the metal center are highly unstable under ambient conditions. The existence of square pyramidal and pseudo-octahedral nitrido-iron species under cryogenic conditions has been deduced from early resonance Raman spectra[21] or from a detailed spectral analysis of their decomposition products.[22−24] Recently, the preparation of a first pseudo-octahedral iron complex with an oxidation state of +6 at the metal center was accomplished in a frozen acetonitrile matrix at 77 K.[25] In this effort, the terminal Fe−N triple bond was stabilized by embedding the metal into an acetate-functionalized cyclam moiety (1,4,8,11-tetraazacyclotetradecane-1-acetate or simply cyclam-ac) serving as a pentadentate ligand, L_5.

For introducing the nitride ligand into the coordination sphere of the metal, a photochemical route was proposed and successfully applied under cryogenic conditions.[13,22,23] Irradiation of a precursor complex containing an axial azide ligand leads to heterolytic N−N bond cleavage and elimination of dinitrogen thereby formally photooxidizing the metal center:

$$[L_5\text{Fe}^n(\text{N}_3)]^+ + h\nu \rightarrow [L_5\text{Fe}^{n+2}\text{N}]^+ + \text{N}_2 \quad (1)$$

For this scheme to succeed, the photolysis wavelength has to be chosen with great care. This is because photooxidation may compete with photoreduction through elimination of azide radicals

$$[L_5\text{Fe}^n(\text{N}_3)]^+ + h\nu \rightarrow [L_5\text{Fe}^{n-1}]^+ + \text{N}_3 \quad (2)$$

or with the elimination of azide anions[26,27]

Received: May 8, 2014
Published: June 20, 2014

   dx.doi.org/10.1021/ja5045133 | J. Am. Chem. Soc. 2014, 136, 10095−10103

$$[L_5Fe^n(N_3)]^+ + h\nu \rightarrow [L_5Fe^n]^{2+} + N_3^- \quad (3)$$

which leaves the oxidation state at the metal center untouched ("redox-neutral"). We have recently been able to detect for the first time a genuine octahedral iron(V) nitride in liquid solution under ambient conditions and to record its reactivity in real time using step-scan Fourier transform infrared (FTIR) spectroscopy.[28] To this end, a diazide complex bearing a tetradentate cyclam ligand, L_4, at the equatorial positions was photolyzed at 266 nm and the formation of the high-valent iron nitride according to

$$[L_4Fe^{III}(N_3)_2]^+ + h\nu \rightarrow [L_4Fe^{V}N(N_3)]^+ + N_2 \quad (4)$$

was monitored through the appearance of the characteristic vibrational band arising from its remaining azide ligand. The highly oxidized product was found to be formed with a relative quantum yield as high as 80%, to live for a few hundred microseconds only and to react with several substrates at nearly diffusion-limited rates. Photolysis of $[L_4Fe^{III}(N_3)_2]^+$ at longer wavelengths resulted predominantly in the release of azide anions and preservation of the oxidation state at the metal center.[28]

A complementary step-scan FTIR study of the photochemistry of the equivalent monoazide $[L_5Fe^{III}(N_3)]^+$ complex in liquid solution under ambient conditions[26,27] did not provide any evidence so far for photooxidation and formation of the high-valent product $[L_5Fe^{V}N]^+$. Despite representing the precedential in vitro model system for photochemical formation of high-valent iron, only photoreductive and "redox-neutral" azide cleavage could be revealed. Therefore, the questions arise as to whether or not the dinitrogen elimination according to (reaction 1) represents a generic photochemical route to high-valent iron and what factors limit its photochemical efficiency.

More importantly, nothing is known so far about the primary events involved in the photooxidation and the time scales associated with them. Is the dinitrogen elimination a direct dissociation or does it involve non-adiabatic transitions between states of different spin multiplicities? What are the primary quantum yields for N_2 dissociation, and ultimately, how can the competing photochemical pathways be suppressed so as to optimize the photooxidation efficiency? To address these complex issues spectroscopic experiments are urgently needed that are capable to expose directly in the time domain the primary events following the initial absorption of a photon. An ultrafast, i.e., femtosecond, time-resolution is required to also reveal the dynamics occurring in the excited electronic states of the metal complexes and to observe the nascent photochemical products including their internal (electronic, vibrational, and rotational) energy distributions.

To this end, we carried out extensive femtosecond mid-infrared (fs-MIR) spectroscopy of $[(cyclam\text{-}ac)Fe^{III}(N3)]PF_6$ in liquid acetonitrile solution at room temperature with variable-wavelength excitation. Such studies will certainly profoundly enhance our current primitive understanding of the primary events involved in the photochemical route to highly oxidized iron. In the future, they may assist the bioinorganic chemistry community in developing novel synthetic model systems of low molecular weight that are capable of supporting high oxidation states of iron and that may ultimately feature catalytic activities that are similar to those of the inspiring macromolecular systems developed by nature.

RESULTS AND DISCUSSION

Linear Spectroscopy. The absorption spectra in the ultraviolet-to-visible (UV–vis) and mid-infrared (MIR) spectral regions of this complex are shown in Figure 1 together with its molecular structure. The most prominent feature in the electronic spectrum is a distinct, broad, and structure-less resonance in the VIS that peaks at 459 nm and that has been assigned previously to a $N_3^- \rightarrow$ Fe ligand-to-metal charge-transfer band.[29] It was exactly this band that was originally exploited to convert the complex in a frozen matrix into an iron(V) nitride.[23,29] Additional, yet to be assigned features appear in the UV spectrum as shoulders at 305, 280, and 245 nm and as a peak at 214 nm.

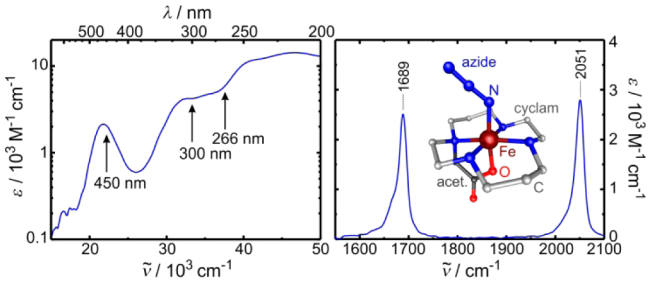

Figure 1. Electronic UV–vis absorption spectrum (left) and FTIR spectrum (right) of $[(cyclam\text{-}ac)Fe^{III}(N_3)]PF_6$ in liquid acetonitrile solution at room temperature. The inset shows the DFT-optimized molecular structure of the complex (H atoms omitted for clarity).

The absorption spectrum of $(cyclam\text{-}ac)Fe^{III}(N_3)^+$ in the mid-IR consists essentially of two resonances originating from the C=O stretching vibration of the acetate group at 1689 cm^{-1} and from the asymmetric N3 stretching vibration of the azide ligand at 2051 cm^{-1}. In this study, these two bands were used to attain time-resolved spectroscopic information about the primary processes following UV–vis excitation of the complex at three different wavelengths, namely at 450, 300, and 266 nm.

VIS Photolysis with fs-MIR Probing. In the fs experiments reported here (for experimental details, see Supporting Information) a solution of the iron azide complex in acetonitrile (MeCN) at room temperature is excited by a UV or a VIS pump pulse and the change of the sample's infrared spectrum in response to this excitation is recorded with a variably delayed broadband mid-IR probe pulse.[30] Such pump-induced fs-MIR spectra are shown in Figure 2a,b for VIS-excitation at 450 nm and for various pump–probe delays ranging from a few hundred femtoseconds up to about 60 ps. To facilitate a comparison of the signal strengths obtained in the two different spectral regions, namely, acetate CO stretching on the one hand and azide stretching on the other, the data are shown alongside an inverted stationary FTIR-spectrum of the complex that was scaled to the maximum bleaching amplitude in the azide stretching region.

In fs-MIR spectra, negative signals can arise because the excitation pulse depletes the electronic ground state of the complex thereby causing a weaker absorbance of the sample at the spectral positions of all ground-state vibrational resonances. Hence, negative signals indicate an effective bleaching of the sample. Accordingly, two such bleaching bands are seen in Figure 2a,b, which spectrally coincide as expected with the two vibrational resonances of the linear FTIR spectrum. Moreover, the amplitude ratio of the two bleaching bands corresponds

dx.doi.org/10.1021/ja5045133 | J. Am. Chem. Soc. 2014, 136, 10095–10103

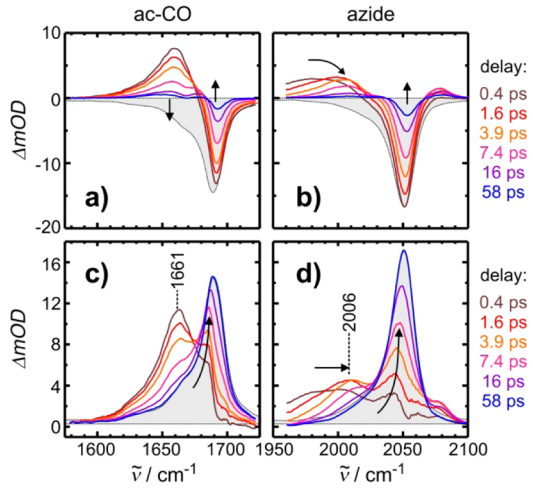

Figure 2. Fs-MIR spectra following 450 nm photolysis of [(cyclam-ac)$Fe^{III}(N_3)$]PF_6 in acetonitrile solution at room temperature in the acetate-CO region (a) and in the azide region (b). The inverted stationary FTIR spectrum that is scaled to the azide bleaching signal at the earliest delay is shown in gray. Subtraction of this spectrum from the fs-MIR data yields purely absorptive fs-MIR "product" spectra (c and d), which gradually evolve into the FTIR spectrum of the equilibrated parent complex (gray).

nicely to the ratio of the peak extinction coefficients for the corresponding pair of linear FTIR resonances. Thus, every photoexcited molecule gives rise to a certain negative signal in the azide region and another, properly scaled, negative signal in the acetate-CO region. These negative bands appear within the time resolution of the experiment and gradually decay with increasing delay in a concerted fashion indicating that the electronic ground state of the complex is dynamically repopulated.

In fs-MIR spectra, positive signals can arise if the frequencies of the vibrational modes of the complex in its electronically excited state are distinctly different from those in the electronic ground state. In addition, such transient absorptions can also arise if the electronic excitation leads to nascent photochemical products whose MIR spectra differ from that of the ground-state complex. According to Figure 2a, such an induced absorption appears markedly downshifted in frequency relative to the ground-state bleach of the acetate-CO region. A complementary frequency-downshifted absorption band is also seen in the azide stretching region (cf. Figure 2b). Thus, we can already conclude that within the time resolution, the optical excitation leaves the internal nuclear structure of the vibrating CO and N_3 absorbing moieties intact.

A spectral analysis of the early time fs-MIR spectrum shows that in the acetate-CO region, the area under the absorption band is about the same as the area under the bleaching band. With increasing time delay, the amplitude of the induced absorption decays while at the same time, the ground-state bleach recovers. Despite being temporally synchronized, bleach recovery and absorption decay do not form a spectrally intermediate isosbestic point. In the azide stretching region (cf. Figure 2b), the time-evolution of the fs-MIR spectrum is considerably more complex. As before, the bleach recovery is accompanied by an overall decay of the downshifted absorption; however, the latter signal also suffers from a subtle time-dependent spectral shift.

To understand the full spectro-temporal evolution in the MIR following VIS-photolysis, it is instructive to derive purely absorptive "product" spectra. To this end, the bleaching contribution can be eliminated by subtracting the properly scaled, inverted FTIR spectrum of the complex from the raw fs-MIR data as shown in Figure 2c,d. Focusing first on the azide region, two distinct absorptions are recovered through this procedure. The frequency-downshifted absorption at early delays appears to be rather broad and to peak around 1980 cm^{-1}. With increasing time delay, it seems to sharpen up and to gradually approach a peak frequency of 2006 cm^{-1}. Apparently, the induced absorption gradually adopts the spectral position of the asymmetric stretching band of free azide anions, which is known to be located in liquid acetonitrile solution at exactly at 2006 cm^{-1}.[26] Thus, we are led to conclude further that upon absorption of a 450 nm photon, the axial azide ligand is dissociated from the metal center, and it is detached as an azide anion. The nascent N_3^- anion is initially formed in a vibrationally excited fashion. The ensuing relaxation of its excess vibrational energy (VER) naturally explains the time-dependent spectral shift and sharpening of the induced absorption. Dynamic solvent reorganization around the nascent anion may also contribute to the spectro-temporal shifting.

The primary dynamics induced upon 450 nm photolysis are illustrated in Figure 3, which sketches schematically the

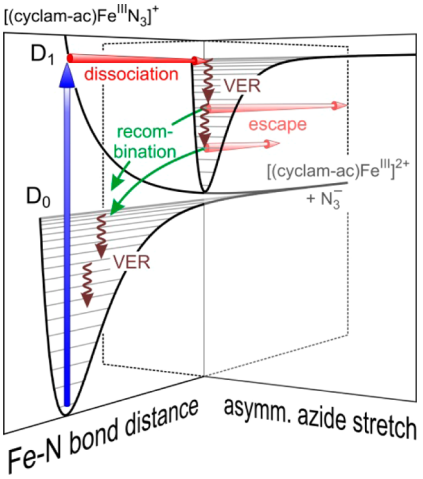

Figure 3. Sketch of the primary processes following 450 nm photolysis of [(cyclam-ac)$Fe^{III}(N_3)$]PF_6 in acetonitrile solution. The parent complex is excited at zero delay with the 450 nm photolysis pulse (vertical arrow). An ultrafast initial dissociation of the Fe−N bond (horizontal arrows) yields a dicationic Fe^{III} complex together with azide anions, which are seen to be formed vibrationally excited and to undergo vibrational energy relaxation (wavy downward arrows). Geminate recombination (curvy downward arrow) partially repopulates the electronic ground state of the parent complex in a vibrationally excited fashion and competes very efficiently with fragment escape (horizontal arrows).

potential energy surfaces of the parent complex as a function of the Fe−N bond distance and the asymmetric stretching coordinate of the azide ligand. Indeed, accompanying calculations based on density functional theory (DFT, see Supporting Information) confirm that the electronic ground state of the complex correlates asymptotically with azide anions and the penta-coordinated dicationic species, [(cyclam-ac)-Fe^{III}]$^{2+}$, in its excited electronic doublet state. The Fe−N bond dissociation energy amounts to ~16000 cm^{-1}, which is more

dx.doi.org/10.1021/ja5045133 | J. Am. Chem. Soc. 2014, 136, 10095−10103

than 6000 cm^{-1} below the energy of the 450 nm photolysis photon.

The second absorption band in Figure 2d is clearly due to the repopulated ground state. At early delays, it peaks at 2043 cm^{-1} and is rather broad, while for later delays it sharpens up and gradually approaches the equilibrium spectral position of the azide stretching vibration of the parent complex. The build-up at 2051 cm^{-1} occurs at the expense of the free N_3^- absorption at 2006 cm^{-1}. These features are a clear spectral signature of the electronic ground state of the parent complex being repopulated in a vibrationally excited fashion[30] upon geminate recombination of the azide anion with the metal-containing, dicationic fragment. Just like the azide anion, the reformed ground state undergoes vibrational energy relaxation, which causes the time-dependent spectral shift and sharpening of its azide ligand stretching absorption.

The "product" spectra in the acetate-CO region are now easily understood: The induced absorption peaking at 1661 cm^{-1} must originate from the acetate-CO stretching mode of the metal containing fragment that has lost the axial azide ligand, i.e., the dicationic complex $[(cyclam\text{-}ac)Fe^{III}]^{2+}$ in its excited electronic doublet state. However, it is possible that its vacant coordination site becomes occupied by a solvent molecule on time scale of about 100 ps (*vide infra*) thereby forming the hexa-coordinated complex $[(cyclam\text{-}ac)\text{-}Fe^{III}(NCMe)]^{2+}$ in its doublet electronic ground state. Due to the geminate recombination, the signal of the fragment complex decays at the expense of an absorption band that gradually approaches the equilibrium spectral position of the acetate-CO stretching vibration of the parent complex. Once again, VER is responsible for a slight spectral shift of the acetate-CO resonance of the nascent ground state.

UV Photolysis with fs-MIR Probing. Having understood the time scales and mechanisms involved in the VIS photolysis, we now focus our attention to the UV-photolysis with pump wavelengths of 300 and 266 nm. The corresponding fs-MIR spectra are shown in Figure 4. At a first glance, the acetate-carbonyl spectral data appear qualitatively similar to those

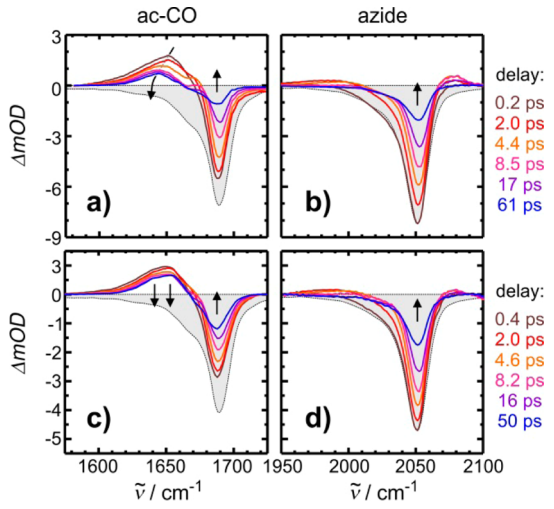

Figure 4. Fs-MIR spectra following 300 nm photolysis (a and b) and 266 nm photolysis (c and d) of $[(cyclam\text{-}ac)Fe^{III}(N_3)]$ PF_6 in acetonitrile at room temperature in the acetate-CO region (a and c) and in the azide region (b and d). The inverted stationary FTIR spectrum that is scaled to the azide bleaching signal at the earliest delay is shown in gray.

measured in the 450 nm photolysis; however, a comparison of the early time spectra with the scaled inverted FTIR spectrum give very strong evidence for the CO-bleaching bands being substantially too weak when the complex is excited in the UV. The amplitude mismatch between the negative signals in the two different spectral regions can only be rationalized by an additional positive signal, which spectrally overlaps with, and thereby diminishes the acetate-CO bleaching band even at the earliest delays. The origin of this additional transient absorption, whose amplitude seems to increase upon shortening the excitation wavelengths (cf. Figure 4a,c), will be addressed shortly.

The complementary data obtained in the azide spectral region at early times upon UV photolysis are markedly different to those obtained with VIS excitation (cf. Figure 4b,d with Figure 2b). Virtually no induced absorption can be detected in the downshifted frequency window near the parent bleach. This can again only be understood if the complex loses—within the time resolution of the experiment—its axial azide ligand. Yet, since no positive signal appears at 2006 cm^{-1}, the azide ligand is evidently not released as an N_3^- anion as was the case in the VIS photolysis. Taking the azide and acetate-CO spectral data together one is led to infer that the UV photolysis leads to elimination of the azide absorber and generates a new species, which gives rise to an additional absorption that spectrally overlaps to a significant extent with the carbonyl bleach of the parent complex.

The subsequent temporal progression of the fs-MIR spectra following UV-excitation reveals as before the concurrent refilling of the two ground-state bleaches. However, significant differences to the VIS photolysis can be noticed in the acetate-CO region. Whereas with 450 nm excitation, the induced absorption was seen to simply decay monotonously and in parallel to the ground-state bleach recovery, the 300 nm photolysis results also in spectral shifting of the positive band. At a delay of 200 fs, the induced absorption peaks at 1651 cm^{-1}, while after 100 ps, it is maximal at 1642 cm^{-1}. This slight dynamic frequency upshift is clearly within the spectral resolution of our instrument. The 266 nm photolysis does not induce such a spectral shifting, but it gives rise to a decaying positive band that peaks around 1660 cm^{-1} and that features a distinct shoulder at 1642 cm^{-1}. These complex findings lend additional credence to the above interpretation of the early time spectra that multiple transient absorptions contribute to the acetate-CO region when the complex is irradiated with UV light.

To obtain further information on the photochemical state of the system following UV absorption, we consult again purely absorptive "product" spectra as shown in Figure 5 for the two characteristic spectral regions and for the two UV excitation wavelengths. Focusing first on the 300 nm photolysis, the product spectrum in the azide region consists only of a single band that is initially very broad and rather weak. With increasing delay, it sharpens up and shifts to lower frequencies. Clearly, these are unmistakable signatures[30] of the vibrationally hot electronic ground state of the parent, which undergoes VER as discussed in the previous section. But, as mentioned before, there is no signature of an azide absorber, neither as an N_3 ligand nor as a free N_3^- anion.

In parallel, the acetate-CO region reveals again the repopulated ground state undergoing vibrational relaxation, but in addition, there is also an extremely broad second absorption that merges on its high-frequency edge with the

dx.doi.org/10.1021/ja5045133 | J. Am. Chem. Soc. 2014, 136, 10095−10103

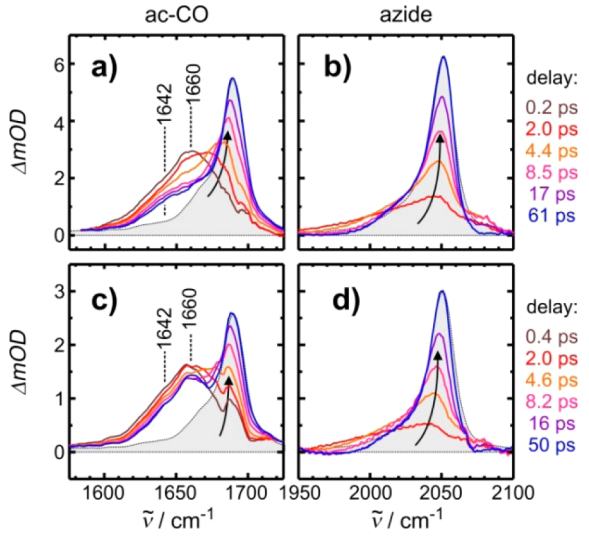

Figure 5. Purely absorptive fs-MIR "product" spectra following 300 nm photolysis (a and b) and 266 nm photolysis (c and d) of [(cyclam-ac)$Fe^{III}(N_3)$]PF_6 in acetonitrile solution at room temperature in the acetate-CO region (a and c) and in the azide region (b and d). The scaled stationary FTIR spectrum of the equilibrated parent complex is shown in gray.

parent absorption band. At early delays, it peaks at ~1660 cm^{-1}, but it evolves into a distinct shoulder around 1642 cm^{-1} for later delays. As alluded to above, these data unequivocally confirm the existence of absorptive signals that spectrally overlap significantly with the ground-state bleach.

Focusing now on the "product" spectra of the 266 nm photolysis, a spectro-temporal evolution is observed in the azide region that is essentially identical to the one recorded with 300 nm excitation pulses (cf. Figure 5b,d). In contrast, pronounced differences to the 300 nm photolysis are noticeable in the acetate-CO region, where apart from the familiar hot ground-state contribution, the additional 1660 cm^{-1}-band featuring the shoulder at 1642 cm^{-1} is again visible. Most strikingly and in stark contrast to the 300 nm photolysis, the ground-state contribution steadily grows in while at the same time, the magnitude of the additional absorption remains more or less constant. Thus, the distinct spectro-temporal evolutions in Figure 5a,c strongly suggest that 300 nm excitation and 266 nm excitation initiate mechanistically different photochemical pathways with different photolysis products. These products can be either unstable with respect to geminate recombination as in the case for excitation at 300 nm or they can be stable on a 100 ps time scale as is the case for excitation at 266 nm. Moreover, we reemphasize that these UV pathways and products are also distinctly different to those originating from the VIS excitation because azide anion absorptions are clearly absent in the fs-MIR spectra of Figures 4 and 5.

UV Photolysis with Step-Scan FTIR Probing. Before assigning the absorptive features seen in Figure 5a,c, it should be kept in mind that all possible photoproducts may still be in a non-equilibrium state even for delays as long as a few picoseconds. This is because on such ultrashort time scales, the products may be dressed with substantial excess vibrational energy (as is clearly the case for the "hot" ground-state, whose absorptions steadily shift to 1689 cm^{-1} and to 2051 cm^{-1} as it continuously relaxes, or for the "hot" azide anion, whose absorption progressively approaches 2006 cm^{-1}) and/or they may be formed in an unrelaxed solvent environment. Therefore, a firm assignment can only be made once these vibrational and solvent dynamics have subsided, i.e., after several tens of picoseconds.

Accordingly, one can use the fs-MIR "product" spectra from Figure 5a,c that were recorded for the longest delays and subtract the equilibrated ground-state contribution peaking at 1698 cm^{-1} (i.e., the gray shaded FTIR spectra). This procedure extracts the spectroscopic signature of all products—other than the replenished and equilibrated ground state—that are still present on a time scale of up to 100 ps and that are apparently able to escape from the geminate recombination. The MIR-absorption of these species (or in short, fs-MIR "escape" spectra) in the acetate-CO region at a delay of 50 ps is displayed in Figure 6a for both UV-photolysis wavelengths, i.e., for 300 nm (dashed) and for 266 nm (gray shaded spectrum).

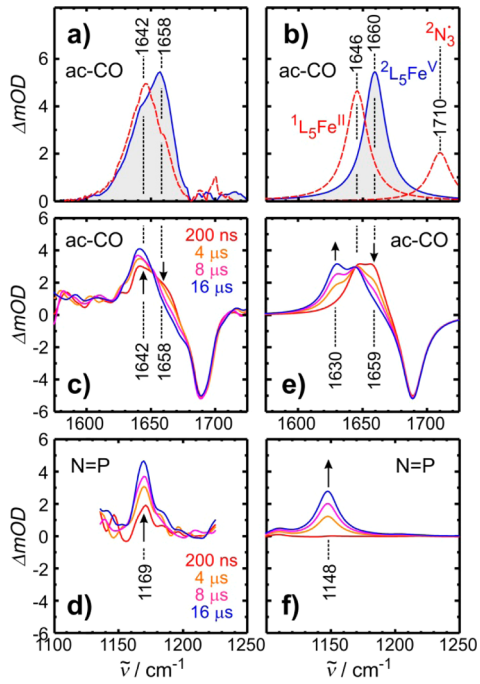

Figure 6. (a) Purely absorptive fs-MIR "escape" spectra in the acetate-CO region following 300 nm photolysis (dashed curve) and 266 nm photolysis (gray shaded). (b) DFT-theoretical infrared "escape" spectra of the high-valent iron(V) nitride (doublet, gray shaded) from the photooxidation pathway and of the low-valent penta-coordinated iron(II) product (quintet) as well as of the azide radical (doublet) from the photoreduction pathway. (c and d) Step-scan FTIR spectra of the quenching experiments with P(*n*Bu)$_3$. (e and f) DFT-theoretical spectra for the quenching reaction 5 converting the iron(V)nitride into the phosphoraniminato-iron(III) complex under pseudo-first-order conditions in the presence of the photoreduction channel. Theoretical frequencies (see Supporting Information) were scaled so as to match the ground-state bleach of the parent. The pseudo1st order rate constant was set to 1/(8 μs), and the branching ratio between photooxidation and photoreduction was assumed to be 0.5.

The "escape" spectrum obtained upon 266 nm photolysis peaks at 1658 cm^{-1} and exhibits the aforementioned distinct shoulder on its low-frequency edge around 1642 cm^{-1}. Interestingly, the "escape" spectrum resulting from the 300 nm photolysis is just a single structureless band peaking at 1642 cm^{-1}, i.e. exactly where the shoulder appears in the 266 nm photolysis. Since azide anions from the redox-neutral Fe—N

dx.doi.org/10.1021/ja5045133 | J. Am. Chem. Soc. 2014, 136, 10095−10103

bond dissociation have not been detected upon UV-photolysis, only very few species can be held responsible for these bands.

In a first scenario, the photoreduction pathway may have opened up, thereby giving rise to the lower-valent monocationic penta-coordinated complex, $[(\text{cyclam-ac})\text{Fe}^{\text{II}}]^+$, and neutral azide radicals.[23] Starting from the optically prepared doublet excited state of the parent complex and provided the nascent azide radicals are born in their doublet ground state, the metal-containing fragment will appear initially in its singlet excited state. In a solid N_2-cryomatrix, the asymmetric stretching mode[31,32] of azide radicals absorb around 1660 cm^{-1}, and the DFT calculations (see Figure 6b) suggest that its transition dipole moment is about a factor of 2 smaller than that of the acetate-CO stretching vibration of the photoreduced complex in its singlet excited state. Subsequent intersystem crossings may lead to the penta-coordinated Fe(II) fragment in its quintet ground state, which lies about 13000 cm^{-1} above the parent doublet ground state. Alternatively, attachment of a solvent molecule (MeCN) may saturate the coordination sphere around the metal center and may give rise to a singlet ground state of the hexa-coordinated species $[(\text{cyclam-ac})\text{Fe}^{\text{II}}(\text{NCMe})]^+$ that is stabilized by ~7000 cm^{-1} with respect to the nascent penta-coordinated fragment and a MeCN molecule. Therefore, if the photoreduction pathway is involved, both of its fragments will show up in the fs-MIR spectra. On a sub-100 ps time scale, these will be most likely the primary products, i.e., ground-state $^2N_3$-radicals and $[(\text{cyclam-ac})\text{Fe}^{\text{II}}]^+$ in its singlet excited state (cf. Figure 6b).

In a second scenario, the photooxidation pathway may have opened up thereby giving rise to the high-valent iron nitride, $[(\text{cyclam-ac})\text{Fe}^{\text{V}}\text{N}]^+$, in its doublet electronic ground state and singlet dinitrogen molecules.[23] The DFT calculations demonstrate that along the N−N bond distance, the doublet electronic ground state of the parent correlates asymptotically with these two products, but photooxidation is hindered by an energy barrier of roughly 14000 cm^{-1} (see Supporting Information). This exit channel lies only 4800 cm^{-1} above the equilibrium structure of ground-state parent complex. Since N_2 is infrared silent, only the metal-containing fragment can contribute to the fs-MIR spectra if the photooxidation pathway is active (see Figure 6b).

The energies of the two UV-photons amount to 33000 and to 38000 cm^{-1}, respectively. Accordingly, both channels (i.e., photooxidation and photoreduction) are energetically accessible. Therefore, an assay is required that is able to differentiate between the high-valent and the low-valent iron species and to discriminate the two alternative photochemical pathways. Along these lines of thoughts, iron(V) nitrides have been shown to act as two-electron nitrogen-atom transfer reagents.[13,18,20] As such they are able to form iron(III) phosphoraniminato complexes upon their bimolecular encounter with phosphorus(III) nucleophiles like tri-*n*-butylphosphane, $P(n\text{Bu})_3$, according to

$$[L_5\text{Fe}^{\text{V}}{\equiv}\text{N}]^+ + P(n\text{Bu})_3 \rightarrow [L_5\text{Fe}^{\text{III}}{-}\text{N}{=}P(n\text{Bu})_3]^+ \quad (5)$$

Reaction 5 has been demonstrated to occur at a nearly diffusion limited rate,[28] but even so, much longer observation times are required than those provided by fs-MIR spectroscopy. Therefore, we have carried out the photolysis of $[(\text{cyclam-ac})\text{Fe}^{\text{III}}(N_3)]PF_6$ in liquid acetonitrile solution at room temperature in the presence of 0.5 equiv P(*n*Bu)3 while the MIR response of the sample was monitored in real time from 200 ns to several microseconds with step-scan FTIR spectroscopy.

In Figure 6c,d, the results of these quenching experiments are shown for the 266 nm photolysis. Despite its inferior signal-to-noise ratio, the step-scan FTIR spectrum recorded in the azide stretching region after 200 ns is in excellent agreement with the fs-MIR spectrum recorded after 50 ps (data not shown). It can clearly be seen that addition of the phosphane diminishes with increasing delay the induced absorption at 1658 cm^{-1}, i.e., exactly where the 100 ps "escape" spectrum of the 266 nm photolysis is maximal. Simultaneously, a new absorption appears in the fingerprint region at 1169 cm^{-1}, which is an unmistakable signature of an N=P double bond stretching vibration of the iron(III) phosphoraniminato complex from reaction 5. This assignment is fully corroborated by our complementary DFT calculations (see Figure 6e,f). When carrying out the step-scan FTIR quenching experiments with longer photolysis wavelengths, neither a buildup of an N=P stretching absorption nor a reduction of the induced absorption in the acetate-CO region were detected within the signal-to-noise ratio.

These findings give very clear evidence that the 266 nm photolysis yields the high-valent iron(V) nitride photoproduct, which in turn exhibits a MIR absorption band due to its acetate-CO ligand that is maximal at 1658 cm^{-1}. Having identified the IR-absorption of the photooxidized product, the absorption band revealed by the MIR "escape" spectrum of the 300 nm photolysis must then be assigned to vibrational modes of the products that are released by the photoreduction pathway; in particular, to the acetate-CO stretching vibration of $[(\text{cyclam-ac})\text{Fe}^{\text{II}}]^+$ and the asymmetric stretching vibration of $N_3^{\bullet}$. The absorption band is very broad and can easily accommodate two unresolved vibrational resonances. Within this notion, the azide radical absorbs on the high-frequency edge of the "escape" spectrum around 1660 cm^{-1} as it does in the solid-state cryogenic matrix,[31,32] while the dominant component at 1642 cm^{-1} is due to the low-valent $[(\text{cyclam-ac})\text{Fe}^{\text{II}}]^+$ complex in its singlet excited state as discussed above. A comparison between the theoretical and the experimental "escape" spectra from Figure 6a,b shows that the chosen DFT-method has its limitations in correctly predicting the vibrational frequency of the various species; in particular of the azide radical.

The time-dependent spectral downshift of the induced absorption seen in Figure 4a is likely to have its origin in the dynamic solvation of the photoreduction fragments and, in particular, in the binding of an acetonitrile molecule by the vacant axial coordination site at the metal center that is left behind by the departing azide radical. A similar, albeit much weaker, time-dependent shift to higher probe frequencies is also observed for the acetate-CO stretching band of the metal-containing fragment that originates from the redox-neutral azide anion cleavage induced upon 450 nm photolysis (cf. Figure 2a). According to the DFT calculation, acetonitrile binding appears to be a complex process that might require preceding non-adiabatic transitions or might even induce such hoppings between states of different spin multiplicities such as quintet and singlet states in the case of Fe(II) or between quartet and doublet states in the case of Fe(III) (see Supporting Information). The process of solvent binding to the coordinatively unsaturated $Fe(CO)_4$ complex, which was prepared upon photolysis of $Fe(CO)_5$, has been studied previously,[33] and quite similar frequency shifts of the carbonyl stretching modes could be detected.

dx.doi.org/10.1021/ja5045133 | J. Am. Chem. Soc. 2014, 136, 10095−10103

We close this section by pointing out again that the 1658 cm^{-1} band of the iron(V) nitride from the 266 nm photolysis exhibits a distinct shoulder at 1642 cm^{-1}, which spectrally coincides with the "escape" spectrum of the photoreduction pathway. Therefore, and in light of the step-scan FTIR quenching experiments, this shoulder strongly suggests that the 266 nm photolysis opens up the photooxidation pathway as an additional channel that has to compete with photoreduction. The latter is already open at much lower excitation energies as evidenced by the spectroscopic results of the 300 nm photolysis. The photoinduced mechanisms for the (cyclam-ac)$Fe^{III}(N_3)^+$ parent complex in acetonitrile solution at room temperature are summarized in Figure 7 for the three excitation wavelengths studied in this paper.

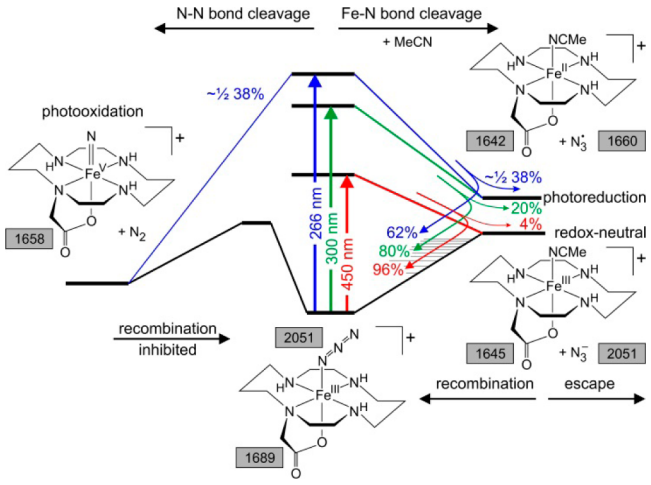

Figure 7. Photochemical pathways of the UV−vis photolysis of (cyclam-ac)$Fe^{III}(N_3)^+$ in acetonitrile solution under ambient conditions. The numbers in gray boxes indicate the vibrational wavenumbers in cm^{-1} of the azide and acetate-CO stretching modes of the various species.

Primary Photoconversion Yield. We finally address the efficiency of the various photochemical pathways. To this end, we return to the negative azide and acetate-CO bleaching signals of the parent complex and study their dynamic recovery as shown in Figure 8. The amplitudes of these bands were recorded at their peak frequency as a function of the pump−probe time delay. The bleaches were found to recover on a time scale of <100 ps in a multiexponential fashion (cf. Figure 8c,d). All signals have in common a dominant exponential component that is characterized by a time constant of ~13 ps. A faster component decays with a time constant of about 2 ps and is also seen in all bleaching signals. The time dependence of the bleach recovery contains all primary processes that replenish the equilibrated electronic ground-state of the complex including all non-adiabatic transitions, geminate recombinations, and vibrational relaxation processes that may occur.

Most importantly, the two exponentials lead asymptotically to a residual bleaching amplitude at infinite delays. This stationary offset signal reflects the fact that the electronic ground state of the cation complex is not quantitatively recovered on time scales even as long as 1 ns. This is because, as mentioned in the previous section, the excitation pulse leaves behind a quasi-permanently perturbed sample in which a fraction of the photoexcited complexes are photochemically converted. The photochemical products as a function of the

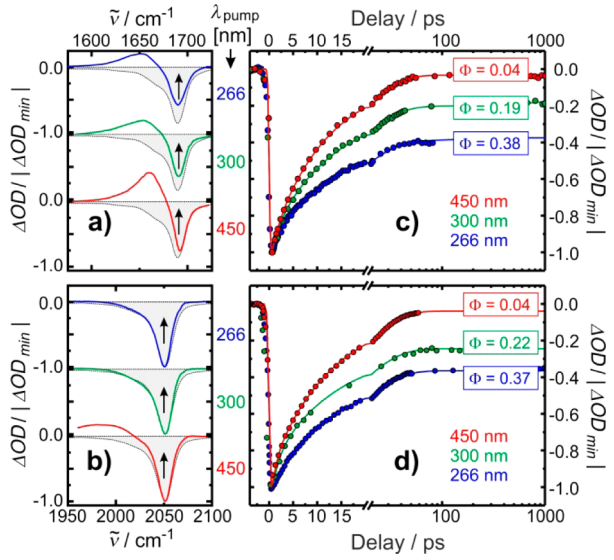

Figure 8. Early time fs-MIR spectra (a and b) and dynamic recovery of the normalized ground-state bleaching signals measured at their peak frequencies (c and d) for the acetate-CO (a and c) and the azide stretching (b and d) regions following UV−vis photolysis of (cyclam-ac)$Fe^{III}(N_3)^+$ in acetonitrile solution under ambient conditions. The vertical arrows in a and b indicate the probing frequencies at which the bleach recovery was recorded as a function of the pump−probe delay. The spectra in a and b were normalized to the maximum bleaching amplitude of the azide stretching band around a time delay of zero.

photolysis wavelengths have been identified from the fs-MIR spectra as well as from the escape spectra discussed above. Quantitative information about the efficiency with which the electronic ground state of the parent complex is recovered through geminate recombination can directly be extracted from these data. Since the vibrational relaxation dynamics of the hot ground state are completed within 1 ns, the asymptotic bleaching amplitude at quasi-infinite time delay relative to the maximum bleach around zero time delay corresponds to the probability, Φ, that the photolysis products escape from their geminate recombination or equivalently, to an upper limit for the quantum yield for photochemical conversion. Note that non-geminate recombination of the primary photolysis products in the homogeneous bulk solution can also occur and may further reduce the photochemical conversion yields on typical time scales of microseconds to milliseconds.

A comparison of the data shown in Figure 8c,d demonstrates that for a given photolysis wavelength, the quantum yields obtained from the acetate-CO bleach are consistent with those extracted from the azide bleach. Yet, the most significant information obtained from the time-dependent signals is that the quantum yield for photochemical conversion depends strongly on the photolysis wavelength. For excitation far in the UV, more than one-third of all photoexcited complexes do not return to the equilibrated ground state. In contrast, for visible excitation into the putative LMCT band this fraction is reduced to merely 4%. Thus, it can be concluded that the photochemical conversion yield increases monotonically with increasing photon energy of the photolyzing radiation. These values are also added to the photochemical pathways sketched in Figure 7.

On the one hand, the data reported here for the photolysis of (cyclam-ac)$Fe^{III}(N_3)^+$ in liquid solution are consistent with the early work of Wieghardt and co-workers,[23] where the 300 nm

dx.doi.org/10.1021/ja5045133 | J. Am. Chem. Soc. 2014, 136, 10095−10103

photolysis was carried out in a photostationary fashion using a Hg immersion lamp and where the photoreduction pathway was also identified. On the other hand, our data are also in stark contradiction to the steady-state photochemistry in the solid-state cryomatrix,[23] where oxidation to the iron(V) nitride was found to be extraordinarily efficient upon illumination of the LMCT band with a conversion yield of up to 80%. It was argued in ref 23 that in contrast to the liquid solution, the solid matrix suppresses the photoreduction channel by enhancing the recombination of the Fe(II) complex with the azide radicals thereby leaving open only the photooxidation pathway.

Our data clearly do not support such reasoning. First, only the oxidation-state preserving pathway to azide anions and the dicationic Fe(III) species is open at an excitation wavelength of 450 nm. Second, the photoreduction channel opens up only when states are prepared that are energetically located above the LMCT state. Third, the geminate recombination occurs almost quantitatively upon LMCT illumination even in the liquid phase, and it is highly probable that non-geminate recombination causes the photochemical conversion to vanish completely when the complex is excited in the VIS region. However, it could very well be that upon dissociation and recombination in the solid-state matrix under continuous irradiation, a small fraction of the parent complexes become transiently trapped in the higher-lying quartet and sextet states. These may live long enough to absorb a second VIS photon thereby further raising the internal energy of the complex to the threshold for photooxidation and even beyond. Thus, the continuous irradiation can lead to an accumulation of the iron(V) nitride in the solid matrix, which cannot occur in laser flash photolysis experiments, where a fresh sample is irradiated with every ultrashort light pulse and where the complex cannot absorb two successive photons.

CONCLUSIONS

In summary, we have studied the primary processes involved in the photochemistry of the complex cation, (cyclam-ac)-$Fe^{III}(N_3)^+$, using femtosecond UV−vis pump MIR-probe spectroscopy and nanosecond step-scan FTIR spectroscopy. The photochemistry is composed of three distinct pathways: (i) the redox-neutral Fe−N cleavage, (ii) the reductive Fe−N cleavage, and (iii) the oxidative N−N cleavage. At the lowest excitation energies, only pathway (i) leading to detachment of an azide anion from the metal center is open. Increasing the excitation energy opens up next the pathway (ii) that gives rise to the detachment of neutral azide radicals while formally reducing the metal center from the oxidation state +3 to +2. As evidenced through quenching experiments, the pathway (iii) opens up only at the highest excitation energies and leads to the intriguing iron(V) nitride through N−N bond dissociation. This photooxidation remains nonetheless a rather inefficient route to high-valent iron because it has to compete with geminate recombination in addition to photoreduction. An upper limit for the primary photooxidation yield of 38% can be extracted from the fs-MIR spectra reported here.

Importantly, all three photodissociations including the iron(V) nitride formation are ultrafast in nature and occur within the time resolution of our experiment of roughly 200 fs. This finding indicates that both the Fe−N and the N−N bond breakages are direct processes that do not require any preceding non-adiabatic transition. Geminate recombination of the fragments and vibrational relaxation of the replenished parent ground state occurs on a slower time scale of about 12 ps and concludes the primary photochemistry of (cyclam-ac)$Fe^{III}(N_3)^+$. More sophisticated electronic structure calculations including molecular dynamics simulations are required to fully understand finer details of the photoinduced dynamics including the influence of potential energy curve crossings and the role of the solvent for the time-dependent vibrational spectroscopy of this fascinating iron complex.

ASSOCIATED CONTENT

Supporting Information

Experimental details. Table summarizing the energetics connected with the photochemical pathways of (cyclam-ac)$Fe^{III}(N_3)^+$ from DFT calculations. DFT-optimized structures and theoretical vibrational spectra of the parent and product complexes. This material is available free of charge via the Internet at http://pubs.acs.org.

AUTHOR INFORMATION

Corresponding Authors

dschwar@gwdg.de

p.voehringer@uni-bonn.de

Notes

The authors declare no competing financial interest.

ACKNOWLEDGMENTS

We gratefully acknowledge financial support by the Deutsche Forschungsgemeinschaft through the Collaborative Research Center 813 “Chemistry at Spin Centers”.

REFERENCES

(1) Shaik, S.; de Visser, S. P.; Kumar, D. *J. Biol. Inorg. Chem.* **2004**, *9*, 661−668.
(2) Denisov, I. G.; Makris, T. M.; Sligar, S. G.; Schlichting, I. *Chem. Rev.* **2005**, *105*, 2253−2277.
(3) Shaik, S.; Kumar, D.; de Visser, S. P.; Altun, A.; Thiel, W. *Chem. Rev.* **2005**, *105*, 2279−2328.
(4) Costas, M.; Chen, K.; Que, L., Jr. *Coord. Chem. Rev.* **2000**, *200*, 517−544.
(5) Costas, M.; Mehn, M. P.; Jensen, M. P.; Que, L., Jr. *Chem. Rev.* **2004**, *104*, 939−986.
(6) Merkx, M.; Kopp, D. A.; Sazinsky, M. H.; Blazyk, J. L.; Muller, J.; Lippard, S. J. *Angew. Chem., Int. Ed.* **2001**, *40*, 2782−2807.
(7) Ferraro, D. J.; Gakhar, L.; Ramaswamy, S. *Biochem. Biophys. Res. Commun.* **2005**, *338*, 175−190.
(8) Geng, C. Y.; Ye, S. F.; Neese, F. *Dalton Trans.* **2014**, *43*, 6079−6086.
(9) Rittle, J.; Green, M. T. *Science* **2010**, *330*, 933−937.
(10) Groves, J. T. *J. Inorg. Biochem* **2006**, *100*, 434−447.
(11) Saouma, C. T.; Peters, J. C. *Coord. Chem. Rev.* **2011**, *255*, 920−937.
(12) Hohenberger, J.; Ray, K.; Meyer, K. *Nat. Commun.* **2012**, *3*, 720.
(13) Smith, J. M.; Subedi, D. *Dalton Trans.* **2012**, *41*, 1423−1429.
(14) Yandulov, D. V.; Schrock, R. R. *Science* **2003**, *301*, 76−78.
(15) Schrock, R. R. *Acc. Chem. Res.* **2005**, *38*, 955−962.
(16) Betley, T. A.; Peters, J. C. *J. Am. Chem. Soc.* **2004**, *126*, 6252−6254.
(17) Rohde, J. U.; Betley, T. A.; Jackson, T. A.; Saouma, C. T.; Peters, J. C.; Que, L. *Inorg. Chem.* **2007**, *46*, 5720−5726.
(18) Scepaniak, J. J.; Fulton, M. D.; Bontchev, R. P.; Duesler, E. N.; Kirk, M. L.; Smith, J. M. *J. Am. Chem. Soc.* **2008**, *130*, 10515−10517.
(19) Vogel, C.; Heinemann, F. W.; Sutter, J.; Anthon, C.; Meyer, K. *Angew. Chem., Int. Ed.* **2008**, *47*, 2681−2684.
(20) Scepaniak, J. J.; Vogel, C. S.; Khusniyarov, M. M.; Heinemann, F. W.; Meyer, K.; Smith, J. M. *Science* **2011**, *331*, 1049−1052.

(21) Wagner, W. D.; Nakamoto, K. *J. Am. Chem. Soc.* **1989**, *111*, 1590−1598.
(22) Meyer, K.; Bill, E.; Mienert, B.; Weyhermüller, T.; Wieghardt, K. *J. Am. Chem. Soc.* **1999**, *121*, 4859−4876.
(23) Grapperhaus, C. A.; Mienert, B.; Bill, E.; Weyhermüller, T.; Wieghardt, K. *Inorg. Chem.* **2000**, *39*, 5306−5317.
(24) Krahe, O.; Neese, F.; Engeser, M. *ChemPlusChem.* **2013**, *78*, 1053−1057.
(25) Wieghardt, K.; Berry, J. F.; Bill, E.; Bothe, E.; George, S. D.; Mienert, B.; Neese, F. *Science* **2006**, *312*, 1937−1941.
(26) Torres-Alacan, J.; Krahe, O.; Filippou, A. C.; Neese, F.; Schwarzer, D.; Vöhringer, P. *Chem.—Eur. J.* **2012**, *18*, 3043−3055.
(27) Vennekate, H.; Schwarzer, D.; Torres-Alacan, J.; Krahe, O.; Filippou, A. C.; Neese, F.; Vöhringer, P. *Phys. Chem. Chem. Phys.* **2012**, *14*, 6165−6172.
(28) Torres-Alacan, J.; Das, U.; Filippou, A. C.; Vöhringer, P. *Angew. Chem., Int. Ed.* **2013**, *52*, 12833−12837.
(29) Aliaga-Alcalde, N.; DeBeer George, S.; Mienert, B.; Bill, E.; Wieghardt, K.; Neese, F. *Angew. Chem., Int. Ed.* **2005**, *44*, 2908−2912.
(30) Reichardt, C.; Schroeder, J.; Vöhringer, P.; Schwarzer, D. *Phys. Chem. Chem. Phys.* **2008**, *10*, 1662−1668.
(31) Tian, R.; Facelli, J. C.; Michl, J. *J. Phys. Chem.* **1988**, *92*, 4073−4079.
(32) Zhou, M. F.; Andrews, L. *J. Phys. Chem. A* **2000**, *104*, 1648−1655.
(33) Portius, P.; Yang, J.; Sun, X.-Z.; Grills, D. C.; Matousek, P.; Parker, A. W.; Towrie, M.; George, M. W. *J. Am. Chem. Soc.* **2004**, *126*, 10713−10720.